Robust Torque Control of Internal Permanent Magnet Motor Using Experimental Flux Maps

Robust Torque Control of Internal Permanent Magnet Motor Using Experimental Flux Maps

Ettore Bianco
Politecnico di Torino
Turin, Italy
ORCID:0000-0003-3653-1893

Fabio Mandrile
Politecnico di Torino
Turin, Italy
ORCID: 0000-0002-7769-8078

Massimiliana Carello
Politecnico di Torino
Turin, Italy
ORCID: 0000-0003-2322-0340

Radu Bojoi
Politecnico di Torino
Turin, Italy
ORCID: 0000-0001-7480-5862

***Abstract*—As the industrial and transportation fields are moving towards electrification, electrical motors are facing increasingly stringent requirements, resulting in accelerated degradation due to parameter variation and component aging. This paper proposes an advanced electric motor torque control strategy robust against the motor parameter variations due to environment and aging. Therefore, to mitigate the adverse effects of these variations, the proposed control strategy leverages multidimensional lookup tables to generate the current references for a standard current vector control. In particular, this paper investigates the impact of motor parameter variations on traditional torque control methods and compares them with a new robust control strategy. The results demonstrate the importance of robust control techniques in electric motor control systems, particularly in demanding applications such as automotive and motorsport.**

Keywords—IPM motor, Flux Maps, FOC 5D, Torque Control, Parameters Variation, Automotive Applications, Cooling Fault.

I. INTRODUCTION

In recent years, there has been a significant interest in the development and implementation of advanced motor torque control strategies to achieve precise and efficient control of electrical motors, such as Direct Flux Control (DFC) [1],[2], Flux Polar Control (FPC) [3], Direct Torque Control (DTC) [4], Field Oriented Control (FOC) [5],[6]. Developing a robust control strategy is particularly important in demanding applications, such as automotive [7]-[10] where the motors are subject to non-negligible parameter variations. Motor parameter variation refers to the changes in motor characteristics such as winding resistance, inductance, and permanent magnet flux due to environment or aging.

Traditional motor torque control techniques, such as Field-Oriented Control (FOC), have been widely used to achieve accurate torque control in electrical motors. However, these techniques are sensitive to motor parameter variations, leading to reduced performance, stability and efficiency [11]. Therefore, it is important to develop advanced control algorithms that can effectively handle parameter variations and maintain accurate torque control despite these variations.

This paper presents a robust electric motor torque control, based on traditional FOC using Current Vector Control (CVC) robust against motor parameter variation. The proposed algorithm is based on multidimensional Lookup Tables (nD-LUT). The nD-LUT are generated through experimental motor flux maps of an Internal Permanent Magnet motor (IPM) for traction applications, able to output the correct references to the FOC under parameter variations.

Besides, the impact of motor parameter variation on the performance and efficiency of the proposed torque control has been analyzed and compared with the FOC 4D proposed in [12]-[15]. The main contributions of this study are the expansion of the 4D LUTs dimensions presented in [13] with the maximum current limit variation. The maximum motor current is variable in automotive applications due to the battery pack current limit, motor current limit at different temperatures, and maximum current derating for motor overload operation. It's not possible to follow strictly the current limit by a simple torque limitation because the correlation between the current and torque can be inaccurate with the parameter variations and in the flux weakening region, in which the current increases to generate flux against the one of the magnets in d-axis.

In the proposed control, the maximum current limit input has been added to the control obtaining 5D LUTs to generate d and q current references for the CVC. In Section II, the proposed FOC 5D control is discussed and described through the proposed control scheme, the operation principles, and then the FOC 5D maps computation process is described. In Section III the simulation results are reported comparing the FOC 4D current limitation possibility with a proper current limitation performed by the FOC 5D. Furthermore, the FOC 5D reaction to a cooling fault has been simulated to underline the possible fault-tolerant behavior of the proposed control. In Section IV the paper conclusions are written demonstrating the FOC 5D superiority for applications with a variable motor current limit.

II. THE FOC 5D CONTROL

In this section, the proposed control is described and its implementation in automotive applications is presented. This type of control has a general nature and it is based on LUTs computed for each different motor to be controlled.

A. FOC 5D Control Scheme and Operation Principles

The control proposed is based on the well-known FOC using CVC, in which the d and q current references are generated for every operating point by two torque-speed LUTs. Instead of traditional FOC, 5D-LUTs have been generated to obtain more precise current references depending on torque reference, estimated speed, magnets' temperature, dc-link voltage and motor current limit. Having three sets of two-dimensional LUTs, three interpolations are required to

generate the current references from the five control inputs. Generated the current references, the CVC control is performed in d and q axes.

The developed motor control is summarized in the block scheme of Fig. 1. The control has 5 inputs: the torque reference T^*, the estimated magnets' temperature T_m, the DC-link voltage v_{dc}, the rotor speed feedback ω, and the current limit i_{max} according to (1) and (2).

$$i_d^* = LUT_{i_d}(T^*, T_m, v_{dc}, \omega, i_{max}) \quad (1)$$

$$i_q^* = LUT_{i_q}(T^*, T_m, v_{dc}, \omega, i_{max}) \quad (2)$$

After the 5D LUTs interpolation, the i_d^* and i_q^* current references are fed to a current controller, which generates the voltage references to be applied to the motor, v_d^* and v_q^*. The voltage references obtained are then transformed from d-q references to three-phase references for the inverter PWM modulator and applied to the motor by the inverter.

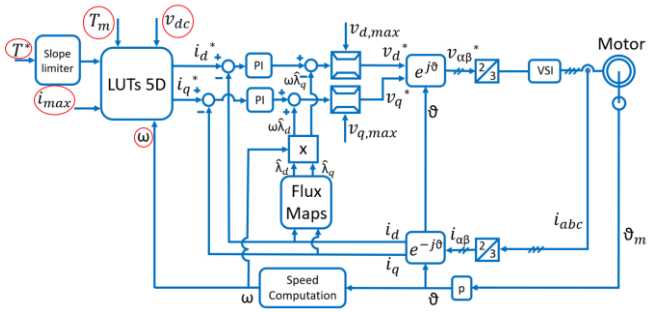

Fig. 1. FOC 5D Control block scheme.

The proposed FOC scheme is a torque control, so the main control input is the torque reference T^*. The speed of the motor ω is retrieved from the motor position sensor with a Phase-Locked Loop (PLL) to obtain a filtered value of the motor speed (speed computation block). The dc-link voltage input v_{dc} is measured by the voltage transducer present in the inverter. Another included input is the magnets' temperature estimated from the motor thermal model [14] and the temperature sensor present on the motor windings. The fifth required input is the maximum motor current limit allowed depending on the lowest current limit from the powertrain components, particularly the battery pack, the inverter and the electric motor, variable with vehicle conditions. The current limit always refers to the maximum current seen by the electric motor. The three added inputs, concerning the conventional FOC, have been included because the temperature affects the motor torque capability [15], the dc-link voltage impacts the flux weakening operation and the maximum current limit can lead to motor damage.

B. Generation of FOC 5D Maps

The proposed motor torque control is based on the motor flux maps. Therefore, a preliminary Finite Element Method Magnetic (FEMM) analysis has been carried out to evaluate the motor maximum limits to be used for bench test design. Later, the flux maps were characterized experimentally for the torque control.

The selected motor was an IPM traction motor, whose parameters are shown in TABLE I. These parameters have been computed by FEMM analysis starting from the motor geometry and materials, because there was no available knowledge of electromechanical motor characteristics.

TABLE I. MOTOR PARAMETERS.

Motor parameter	***Value***	***Unit of Measure***
Number of pole pairs	7	-
Rated power	10	(kW)
Rated current	380	(Apk)
Rated speed	2166	(rpm)
Rated torque	44	(Nm)
Maximum speed	8500	(rpm)
Maximum current	528	(Apk)
Rated dc-link voltage	52	(V)
Phase resistance @ 25°C	11	(mΩ)

The Fig. 2 reports half of the cross-section motor geometry with the materials used for the production: Copper, Iron NO20 for the magnetic core and Neodymium N45SH for the magnets.

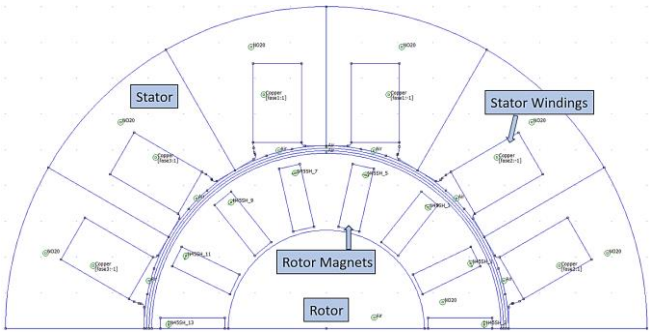

Fig. 2. Motor Geometry and materials for FEMM analysis.

The FEMM analysis outputs are the motor flux maps useful for the control loci evaluation to size the test bench and the regulators tuning for the current vector control. In Fig. 3 the motor flux maps are shown.

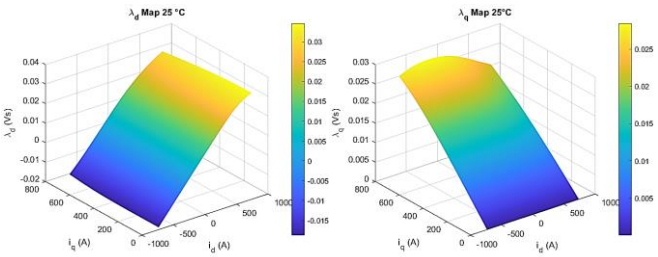

Fig. 3. FEMM motor flux maps in d-axis (left) and in q-axis (right).

In Fig. 4 the Maximum Torque per Ampere (MTPA), the Maximum Current, for transient operation (528 A) and continuous operation (380 A), and the Maximum Torque per Volt (MTPV) control loci are shown.

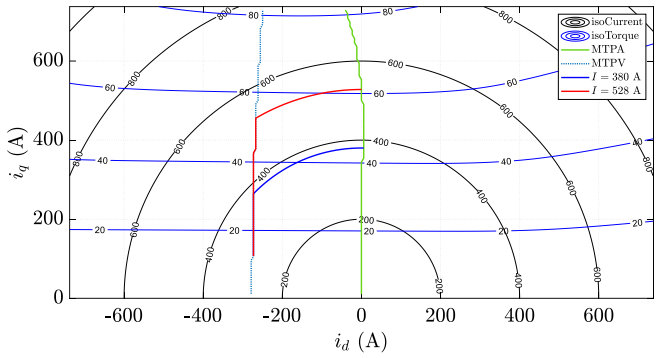

Fig. 4. FEMM motor control loci in motoring operation.

C. *Test bench for experimental flux maps identification*

Having obtained the motor's maximum electromechanical values, the test bench was sized accordingly. The test bench, shown in Fig. 5, consists of the Motor Under Test (MUT), which is current controlled, and a driving motor, which is speed controlled. Both machines are connected onto the same shaft. The imposed speed is typically 1/3 of the motor base speed, in order to make the motor iron losses negligible [16]. The employed acquisition system is the HBM GEN2tB acquiring the three-phase current sensors LEM IT 605-S, the torque meter HBM T40b and the three-phase voltages.

The test procedure consists of a motor-generator-motor sequence to compensate the effect of the resistive voltage drop of the motor, as explained in [16].

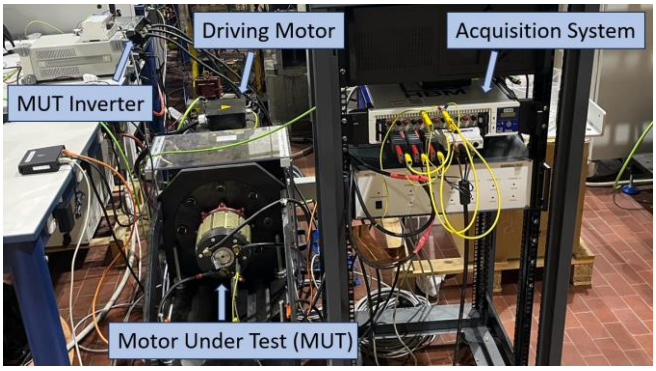

Fig. 5. Test bench setup.

As the torque production is influenced by the permanent magnets' temperature, the test procedure has been repeated at room temperature and at 100°C of magnet temperature obtaining the cold maps (Fig. 6) and the hot maps (Fig. 7). The measured magnets' flux is 0.0148 Vs at 25 °C and 0.0135 Vs at 100°C.

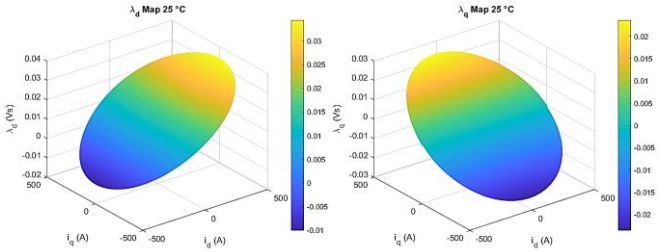

Fig. 6. Cold Flux Maps at 25°C on d-axis (left) and on q-axis (right).

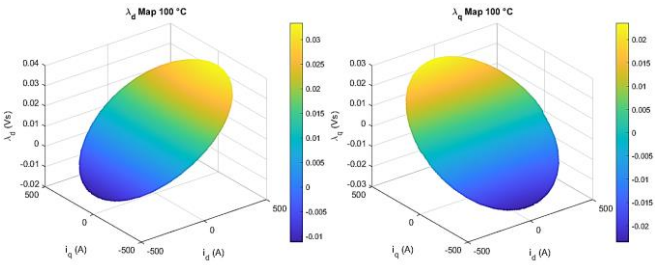

Fig. 7. Hot Flux Maps at 100°C on d-axis (left) and on q-axis (right).

The motor flux maps have been used to compute the optimal control loci for the motor control. In Fig. 8, the control loci, MTPA, MTPV and the iso-Torques, computed from the cold flux maps at 25°C and the hot flux maps at 100°C, are shown.

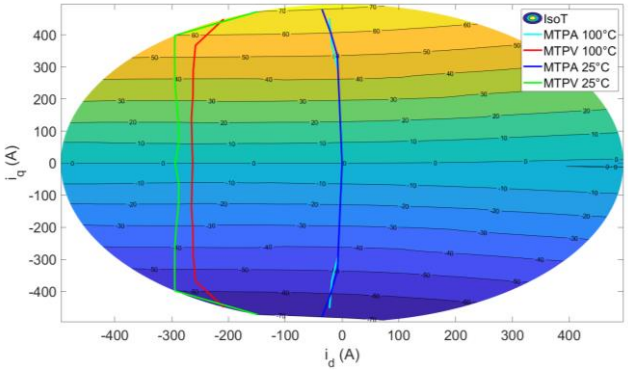

Fig. 8. Motor control loci at 25°C and 100°C.

After the control loci computation, the 5D-LUTs have been computed from the motor flux maps. An example of d and q normalized current maps implemented in the motor control, at 60 V of dc-link voltage, 100 °C of magnets' temperature and 500 Apk of maximum current limit, is shown in Fig. 9 and Fig. 10.

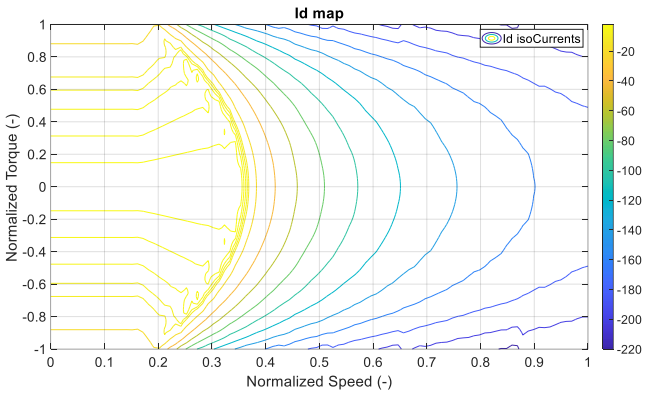

Fig. 9. Normalized Id current map at 60 V, 100 °C and 500 Apk.

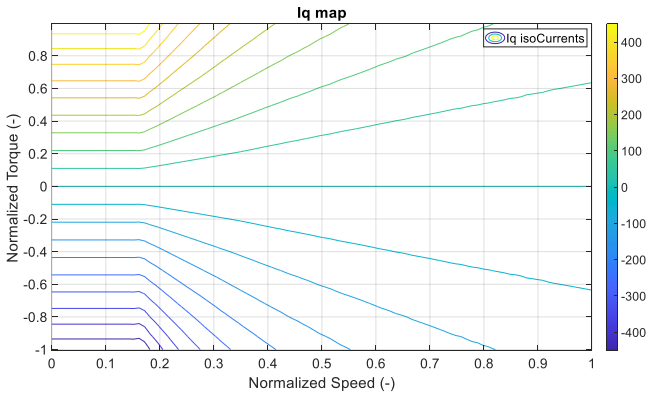

Fig. 10. Normalized Iq current map at 60 V, 100 °C and 500 Apk.

III. Simulation Results

In this section, the effects on the control performance of the FOC 5D strategy are compared with a traditional torque limitation. Besides, the proposed control precision is evaluated under adverse conditions like an instant fault in the cooling system.

A. *Powertrain Components Modeling*

The powertrain components have been modeled using the Simscape electrical library, in particular: the battery pack is modeled as a voltage source and the motor is modeled by the Simscape component for the Voltage Behind Reactance motor as explained in [12]. The motor control code has been properly developed in C language and integrated into the simulation using the MATLAB S-function.

B. *FOC 4D with constant torque limitation*

Typically, to perform a variable current limitation in a well-known FOC or FOC 4D, the conventional solution is to limit the torque according to a fixed relation between torque and current. The main issue of this procedure is the relation between torque and current changes with the magnets' temperature, the motor speed, and the DC-link voltage. The imposed torque limitation is inaccurate under parameters' variation, for example when the temperature is different from the one used to identify the torque-current relation. To understand the temperature effects on current limitation, a simulation test has been performed using a speed of 1000 rpm and a reference torque of 20 Nm. The actual torque, using FOC 4D, follows the reference torque, as shown in Fig. 11.

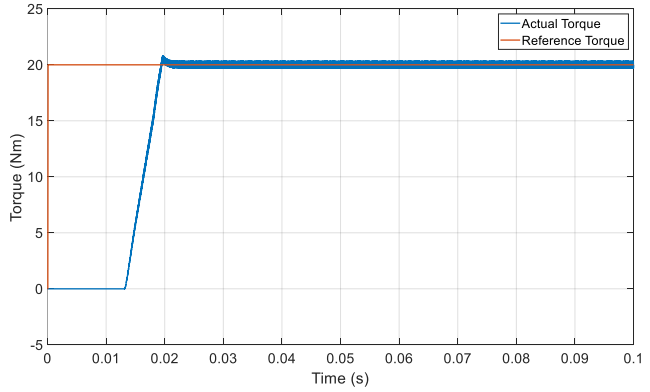

Fig. 11. Torque comparison between reference (red) and actual value (blue).

The simulation has been performed at different temperatures comparing the resultant limitation of the current amplitude obtained as shown in Fig. 12, where it is possible to observe the current limitation difference between the maximum and minimum motor operating temperature. The current difference is due to the control that adjusts the current amplitude to track the correct torque even during temperature variation.

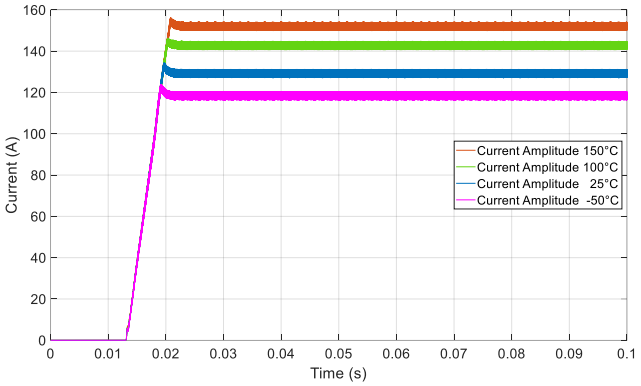

Fig. 12. Current amplitude at different temperatures with the same torque reference of 20 Nm.

The maximum difference obtained was about 40 A, and it is evident that, with this method, the current limit is temperature dependent, so the current error is not negligible. This current limit error is crucial, especially in demanding applications, in which the motor temperature varies significantly and a precise current limit control is mandatory. Using a constant torque limit also in the flux weakening operation, the current limit can be even less accurate at high speed.

A simulation test has been set up with a speed ramp from zero to 7000 rpm, in order to evaluate the current limit behavior at high speed. The torque is fixed at 20 Nm, during the acceleration, up to the flux weakening operation. In Fig. 13-a the torque reference is compared with the simulated actual torque. The current limit trend at high speed, for a constant torque limitation of 20 Nm, is shown in Fig. 13-b. The motor current at low speed is about 140 A, but it increases as the speed increases and the control reaches flux weakening operation, even though the torque decreases. The current limit error is about 100 A at 7000 rpm. At time 0.063 s the motor base speed is reached and the final speed is reached at time 0.085s. Therefore, using the constant torque limitation, the electrical machine current is not limited according to the actual motor thermal constraints, with potentially unacceptable consequences.

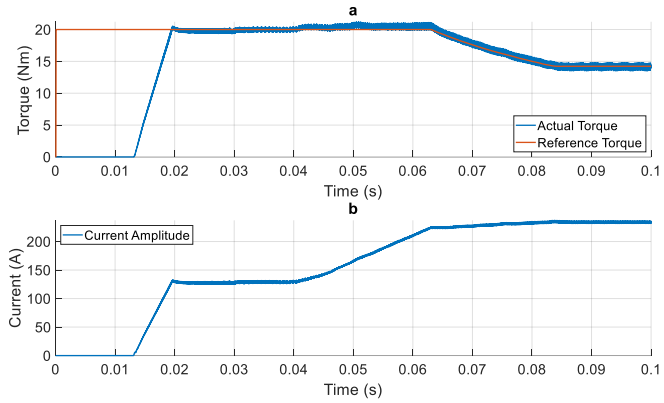

Fig. 13. Torque comparison: reference and actual torque (a) and actual current amplitude (b).

C. *FOC 5D for current limitation*

Due to the impossibility of properly controlling the maximum current through a fixed relation between torque and current, a FOC 5D control has been implemented and the main results are presented in this section. The fifth dimension of the implemented FOC 5D is the motor current limit; the tested current limit is 200 Apk, corresponding to the maximum current of the motor for continuous operation.

The control has been tested with different temperatures, imposing the maximum torque available as reference. The current limit is reached only when the maximum available torque is requested. So, having set the current limit to 200 Apk and requested the maximum torque, the actual torque varies with temperature, as visible in Fig. 14.

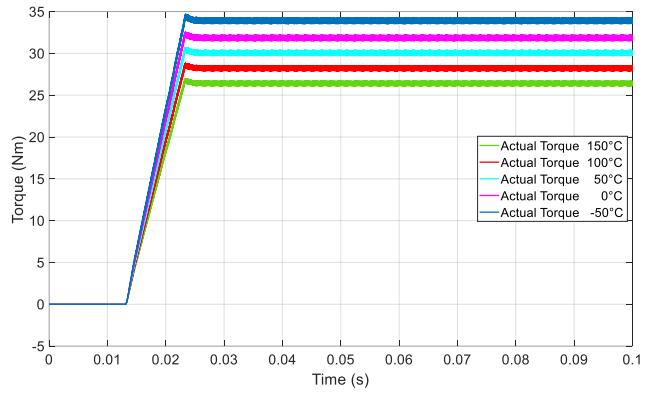

Fig. 14. Maximum torque under temperature variation from -50°C to 150°C with current limitation to 200 Apk.

In correspondence with the maximum current, the FOC 5D computes the maximum torque to have a fixed maximum current amplitude (200 Apk) as visible in Fig. 15.

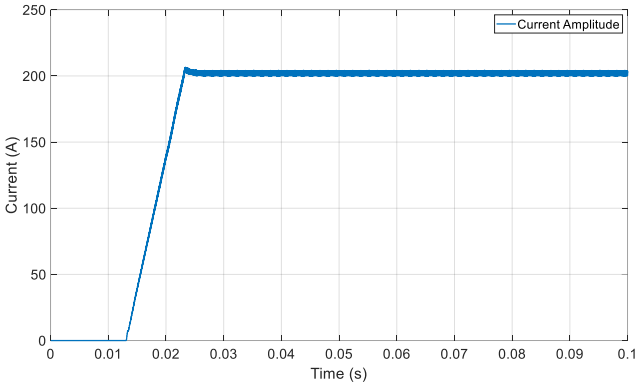

Fig. 15. Maximum current amplitude with FOC 5D implementation.

The high-speed test has been repeated with the FOC 5D control using a maximum current amplitude of 200 Apk. The speed ramp has been limited to 4500 rpm because the motor cannot reach the datasheet maximum speed anymore, with a reduced maximum current.

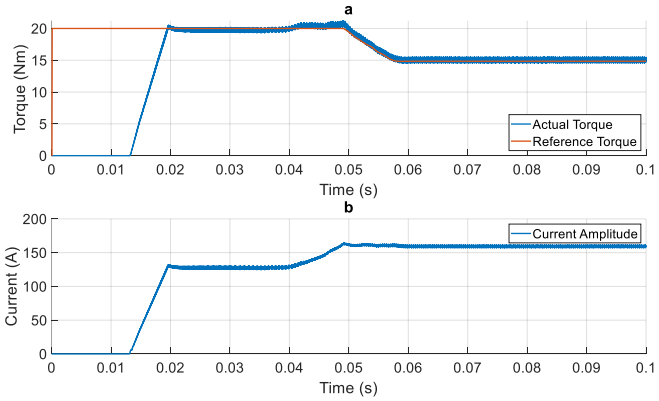

Fig. 16. Torque comparison during a speed ramp from 0 to 4500rpm (a) and current amplitude during flux weakening using FOC 5D for current limit control (b).

The reference torque is 20 Nm and the torque behavior is shown in Fig. 16-a. The actual torque follows accurately the reference at steady state, in the constant torque region the actual torque does not follow strictly the reference because of the speed transient. At time 0.05 s the motor base speed is reached and the final speed is reached at time 0.06 s. The current amplitude that derives from the requested torque is visible in Fig. 16-b. In comparison with the simple torque limitation, in Fig. 13-b, the current amplitude cannot exceed 200 Apk because the FOC 5D limits the current to the maximum one allowed.

D. *FOC 5D during a cooling fault*

The FOC 5D can be seen as a fault-tolerant control and it gives a clear advantage during a fault of the motor cooling. When a cooling fault happens, the motor cooling changes from forced cooling (liquid or air) to natural air cooling, considering the worst case. This section presents the FOC 5D applied on the motor under study during a fault on the fan responsible for the forced air cooling. The maximum current from the motor datasheet has been used to identify the maximum current limits with forced air cooling and natural air cooling. In Fig. 17, the control reaction to a signal, representing the cooling fault event is presented by showing

the worst case when the maximum torque is requested and at time 0.05 s a cooling fault happens.

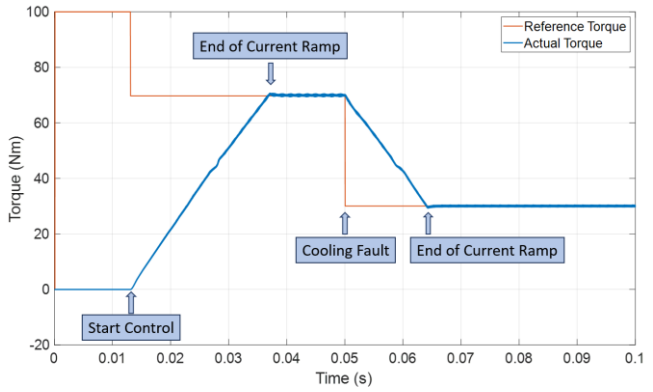

Fig. 17. Torque comparison between reference value (red) and the actual value (blue) using FOC 5D during a cooling fault.

The maximum torque reference is switched instantly from the one that can be obtained considering forced air cooling, to the one considering natural air cooling. The choice of doing a step change between the two torque reference values has been adopted to avoid temperature increase even in the worst case, when the motor winding is at the maximum temperature at thermal steady state and at that time a cooling fault happens. The worst-case thermal condition during a cooling fault is explained considering Fig. 18. During normal operation, the maximum motor electric power is higher respect to the one on fault operation, due to the different heat extraction capabilities. An optimally sized cooling system can guarantee, with the maximum electric power absorption, a maximum temperature on the motor windings below the safety limit. This consideration is valid both for forced air cooling and for natural air cooling, at a thermal steady state, with a maximum winding temperature equal for both cooling types, according to (3)-(5):

$$P_{MaxLoss,Cooling} = P_{Th,Cooling} \tag{3}$$

$$P_{MaxLoss,NoCooling} = P_{Th,NoCooling} \tag{4}$$

$$T_{MaxWinding,Cooling} = T_{MaxWinding,NoCooling} \tag{5}$$

where: $P_{MaxLoss,Cooling}$ are the power losses in normal cooling operation, $P_{Th,Cooling}$ is the extracted power in normal cooling operation, $P_{MaxLoss,NoCooling}$ are the power losses during a cooling fault, $P_{Th,NoCooling}$ is the extracted power during a cooling fault, $T_{MaxWinding,Cooling}$ and $T_{MaxWinding,NoCooling}$ are the winding temperature in normal cooling operation and during a cooling fault, respectively.

To obtain the same maximum winding temperature with a cooling fault, the electric power absorption needs to be reduced due to the reduced heat extraction possibility. So, during a cooling fault in the worst case, the optimal power switch is a step variation, maintaining the winding temperature to the maximum allowed value.

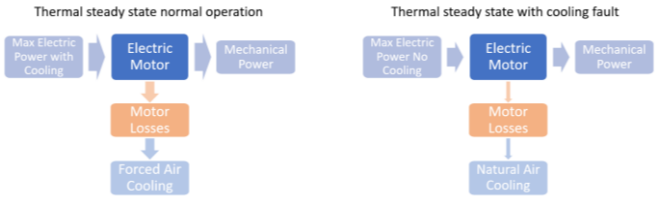

Fig. 18. Thermal power flow during normal operation (left) and during a cooling fault (right).

As emerges from Fig. 18, the optimal torque reference switch is a step change but, due to ramp limitation on the current, the actual torque has a ramp behavior. It is possible to see the same behavior for the current reported in Fig. 19, where it changes from the maximum value allowed at forced air cooling to the maximum value with natural air cooling.

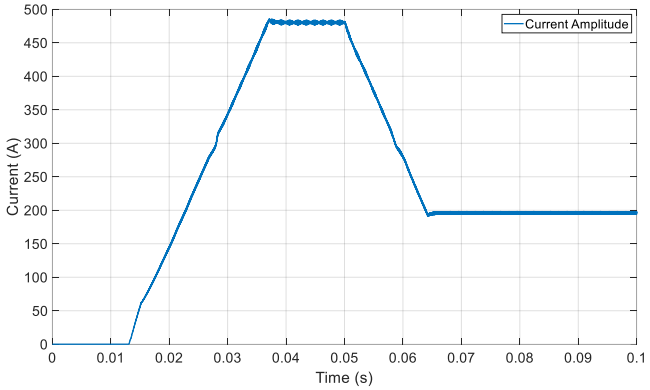

Fig. 19. Current amplitude using FOC 5D during a cooling fault.

The ramp current transition contributes, in the worst case, to the winding temperature increase over the maximum allowed limit. But, in comparison with the motor thermic constant of about 1 h, the current ramp lasts 0.01 s for an associated increase of joule losses of about 250 W, so the associated winding temperature increase is negligible. The 5th LUTs dimension can be also used in short-term motor overload conditions, well-controlling the current amplitude during the derating strategy and keeping the stator winding temperature under the temperature voltage threshold.

IV. Conclusions

This paper presented a novel robust torque control, that has been implemented and compared with the FOC 4D benchmark. The 4D maps of an electric motor have been extended by including a further dimension that takes into account the motor's maximum current limit. The FOC 5D has guaranteed more robustness and precision on the maximum current control in conditions where a current derating is mandatory to avoid motor damage due to overtemperature. The FOC 5D has been developed, first through flux maps from FEMM analysis and then through experimental flux maps. The FOC 5D has been developed in C language, compliant with real-time implementation, using 5-dimensional LUTs to obtain the d and q current references.

The proposed control has been compared with the benchmark in critical conditions when a proper maximum current control is mandatory. It turned out better under parameter variation and in flux weakening operation with a

limited maximum current, keeping the maximum current under the limit.

FOC 5D control has also been tested during a cooling fault, showing that this solution is able to suddenly limit the current compatibly to natural air cooling and so, to avoid the winding temperature increase over the safety limit. The results underline that FOC 5D is more robust in demanding applications like automotive because it contributes to torque control reliability and robustness and reaches higher vehicle reliability, where the motor current limit is strongly variable due to short-time operations, thermal conditions of different powertrain components, battery pack state of charge and environment temperature. Furthermore, the FOC 5D is a fault-tolerant control for cooling issues; the proposed control has been tested under a cooling fault and it has been guaranteed to maintain the motor windings under the maximum temperature limit.

REFERENCES

[1] Pellegrino, G.; Bojoi, R.; Guglielmi, P. Unified Direct-Flux Vector Control for AC motor drives. In Proceedings of the 2010 IEEE Energy Conversion Congress and Exposition, Atlanta, GA, USA, 12–16 September 2010; pp. 1150–1157, doi: 10.1109/ECCE.2010.5617840.

[2] S. Rubino, I. R. Bojoi, E. Armando and A. Tenconi, "Deadbeat Direct Flux Vector Control of Surface Permanent Magnet Motor Drives," in IEEE Transactions on Industry Applications, vol. 56, no. 3, pp. 2685-2699, May-June 2020, doi: 10.1109/TIA.2020.2972835.

[3] Rubino, S.; Tolosano, L.; Mandrile, F.; Armando, E.; Bojoi, R. Flux Polar Control (FPC): A Unified Torque Controller for AC Motor Drives. IEEE Trans. Ind. Appl. 2023, 59, 4140–4163, doi: 10.1109/TIA.2023.3270110.

[4] Meesala, R.E.K.; Athikkal, S.; Pradhan, P.; Prasad, S.; Prasad, A. Modified Direct Torque Control of PMSM Drive for Electric Vehicle Application. In Proceedings of the 2021 IEEE Madras Section Conference (MASCON), Chennai, India, 27–28 August 2021pp. 1–5, doi: 10.1109/MASCON51689.2021.9563576.

[5] Nicola, C.-I.; Nicola, M. Real Time Implementation of the PMSM Sensorless Control Based on FOC Strategy. In Proceedings of the 2022 4th Global Power, Energy and Communication Conference (GPECOM), Nevsehir, Turkey, 14–17 June 2022; pp. 179–183, doi: 10.1109/GPECOM55404.2022.9815684.

[6] Bianco, E.; Rizzello, A.; Ferraris, A.; Carello, M. Modeling and experimental validation of vehicle's electric powertrain. In Proceedings of the 2022 IEEE International Conference on Environment and Electrical Engineering and 2022 IEEE Industrial andCommercial Power Systems Europe (EEEIC/I&CPS Europe), Prague, Czech Republic, 28 June–1 July 2022; pp. 1–6, doi: 10.1109/EEEIC/ICPSEurope54979.2022.9854612.

[7] A. Amerise, M. Mengoni, L. Zarri, A. Tani, S. Rubino and R. Bojoi, "Open-ended induction motor drive with a floating capacitor bridge at variable DC link voltage," 2017 IEEE Energy Conversion Congress and Exposition (ECCE), Cincinnati, OH, USA, 2017, pp. 3591-3597, doi: 10.1109/ECCE.2017.8096638.

[8] De Carvalho Pinheiro, H., Messana, A., Sisca, L., Ferraris, A., Airale, A.G., and Carello, M., "Torque Vectoring in Electric Vehicles with In-wheel Motors," in: Uhl, T., ed., Advances in Mechanism and Machine Science, Springer International Publishing, ISBN 978-3-030-20131-9: 3127–3136, 2019, doi:10.1007/978-3-030-20131-9_308.

[9] Ferraris, A., De Carvalho Pinheiro, H., Galanzino, E., Airale, A.G., and Carello, M., "All-Wheel Drive Electric Vehicle Performance Optimization: From Modelling to Subjective Evaluation on a Static Simulator," 2019 Electric Vehicles International Conference, EV 2019, 2019, doi:10.1109/EV.2019.8893027.

[10] de Carvalho Pinheiro, H.; Punta, E.; Carello, M.; Ferraris, A.; Airale, A. G., Torque Vectoring in Hybrid Vehicles with In-Wheel Electric Motors: Comparing SMC and PID control, 21st IEEE International Conference on Environment and Electrical Engineering and 2021 5th IEEE Industrial and Commercial Power System Europe, EEEIC / I and CPS Europe 2021 - Proceedings, Institute of Electrical and Electronics Engineers Inc., pp. 6, 2021, ISBN: 978-1-6654-3613-7, DOI: 10.1109/EEEIC/ICPSEurope51590.2021.958473.

[11] D. Cittanti, V. Mallemaci, F. Mandrile, S. Rubino, R. Bojoi and A. Boglietti, "PWM-Induced Losses in Electrical Machines: An Impedance-Based Estimation Method," 2021 24th International Conference on Electrical Machines and Systems (ICEMS), Gyeongju, Korea, Republic of, 2021, pp. 548-553, doi: 10.23919/ICEMS52562.2021.9634438.

[12] Bianco, E.; Rubino, S.; Carello, M.; Bojoi, I.R. Advanced Torque Control of Interior Permanent Magnet Motors for Electrical Hypercars. World Electr. Veh. J. 2024, 15, 46. https://doi.org/10.3390/wevj15020046

[13] Trancho, E.; Ibarra, E.; Arias, A.; Salazar, C.; Lopez, I.; de Guerenu, A.D.; Peña, A. IPMSM Torque Control Strategies based on LUTs and VCT feedback for Robust Control under Machine Parameter Variations. In Proceedings of the IECON 2016—42nd Annual Conference of the IEEE Industrial Electronics Society, Florence, Italy, 23–26 October 2016, doi: 10.1109/IECON.2016.7793556.

[14] G. M. El Murr, S. Elkelani Babaa and A. Ordys, "Parameter Identification of IPM Motor Reduced Order Thermal Model for Traction Applications," 2019 1st International Conference on Unmanned Vehicle Systems-Oman (UVS), Muscat, Oman, 2019, pp. 1-6, doi: 10.1109/UVS.2019.8658315.

[15] Y. -S. Kim and S. -K. Sul, "Torque Control Strategy of an IPMSM Considering the Flux Variation of the Permanent Magnet," 2007 IEEE Industry Applications Annual Meeting, New Orleans, LA, USA, 2007, pp. 1301-1307, doi: 10.1109/07IAS.2007.202.

[16] E. Armando, P. Guglielmi, G. Pellegrino and R. Bojoi, "Flux linkage maps identification of synchronous AC motors under controlled thermal conditions," 2017 IEEE International Electric Machines and Drives Conference (IEMDC), Miami, FL, USA, 2017, pp. 1-8, doi: 10.1109/IEMDC.2017.8002334.